

In situ investigations of the electronic properties of coevaporated amorphous Mg-Zn alloy films

Marie-Luce Thèye, Van Nguyen-Van, and Serge Fisson

Laboratoire d'Optique des Solides, Université Pierre et Marie Curie, 4 place Jussieu, F-75230 Paris Cédex 05, France*

(Received 31 July 1984)

Amorphous Mg-Zn alloys have been obtained in the form of thin films by coevaporation under ultrahigh vacuum on cold (≈ 10 K) sapphire substrates, for Zn concentrations between 28 and 35 at. %. These films crystallize at about 350 K. Their dc electrical resistivity and their optical properties between 0.6 and 4 eV have been investigated *in situ*. The resistivity versus temperature behavior is roughly similar to that reported for quenched bulk alloys but the resistivity values are significantly larger. The complex dielectric constant follows the free-electron Drude model at low energies up to 1.8 eV. The optical free-electron parameters are discussed and compared to those obtained on other free-electron-like amorphous alloys. Special attention is paid to the average effective number of conduction electrons per atom, which is found to be smaller than expected.

I. INTRODUCTION

Metallic glasses form an interesting class of new materials, not only because of their unique properties which make them suitable for various applications, but also because they offer a possibility of testing the theoretical models proposed for the effects of disorder in metals. Although most studies up to now have been devoted to systems involving transition metals, amorphous alloys containing only "normal," i.e., free-electron-like metals, like the amorphous Mg-Zn alloys, presently attract increasing interest. This is largely due to the expected relative simplicity of their electronic structure, since the conduction-electron states can be assumed to be almost exclusively of *s* and *p* character. Such a case can be treated theoretically by *ab initio* pseudopotential methods,¹⁻⁴ which succeeded in explaining the constitution diagrams as well as the interrelation between glass formation and phase diagram from a microscopic quantum-mechanical basis. These amorphous alloys are of significant importance from the point of view of the electron transport properties. They have, indeed, relatively low resistivities (of the order of 50–100 $\mu\Omega$ cm), which makes them particularly suited for tests of theories based on the Faber-Ziman theory, initially developed for liquid metals on the basis of the nearly-free-electron model under the assumption of weak scattering, and later on generalized to amorphous metallic alloys.⁵⁻¹⁰

Amorphous Mg-Zn alloys have first been obtained¹¹ by rapid quenching from the melt in a narrow composition range: $25 < x_{\text{Zn}} < 32$ at. % around the deep eutectic (Mg₇₂Zn₂₈). This range has been somewhat extended later on, using the same melt-spinning technique: $22.5 < x_{\text{Zn}} < 35$ at. %.¹² Amorphous Mg-Zn alloys have also been prepared in the form of thin films by a getter-sputtering technique on substrates maintained at 77 K, over a much wider composition range: $10 < x_{\text{Zn}} < 90$ at. %.¹³

The transport properties of amorphous Mg-Zn alloys

prepared by rapid quenching from the melt have been studied in detail over a wide temperature range.¹⁴⁻¹⁷ The results of Hall-effect,¹⁵ electronic specific-heat,¹⁸ magnetic susceptibility,¹⁹ and Compton-profile²⁰ measurements all reveal remarkably good agreement with the predictions of a free-electron model, with Mg and Zn both contributing two electrons per atom to the alloy conduction band. There is, however, some composition dependence of several of these physical quantities, especially in the vicinity of the composition of the crystalline phase Mg₅₁Zn₂₀ ($x_{\text{Zn}} = 28.2$ at. %).¹²

The aim of the present work is to prepare amorphous Mg-Zn alloys in the form of thin films by coevaporation of the two constituents under ultrahigh vacuum onto substrates maintained at low temperature, to measure their transport and optical properties *in situ* as a function of temperature, and to compare the results to those reported for bulk quenched amorphous alloys. Because the two metal constituents, especially Mg, are highly oxidizable materials, coevaporation under ultrahigh vacuum presents the advantage of avoiding contamination of the samples during their preparation. It also allows us to obtain thin films with high-quality surfaces, well adapted to precision optical measurements. Investigations of the optical properties are complementary to those of the transport properties, since they can give information on the conduction-electron behavior in the presence of a high-frequency electromagnetic field; they are particularly useful in that respect since they allow the separate determination of the ratio of the average effective number of electrons per atom *n* to their effective mass *m*, and the relaxation time τ , while dc electrical resistivity measurements only yield the product of these quantities. Optical studies can, on the other hand, bring some insight into the electronic density of states by revealing the existence of interband electron transitions.²¹⁻²³

We present in the following the results obtained on a series of amorphous Mg_{1-x}Zn_x alloy films, with $26 < x_{\text{Zn}} < 35$ at. %, all measurements being performed *in*

situ, under ultrahigh vacuum. In Sec. II we briefly describe the experimental setup, the deposition conditions, and the different experimental techniques. In Sec. III we investigate the variations of the electrical dc resistivity as a function of temperature between 10 and 300 K, and we analyze, on the one hand, the irreversible effects occurring during annealing of the as-deposited films up to 300 K, and, on the other hand, the reversible behavior of the resistivity for annealed (stabilized) amorphous samples. In Sec. IV, we examine the optical properties as deduced from *in situ* reflectance and transmittance measurements from 0.6 to 4 eV on as-deposited films, and we analyze these properties in terms of the free-electron Drude model. We discuss the values of the characteristic parameters of the conduction electrons as a function of composition.

II. PREPARATION AND CHARACTERIZATION OF AMORPHOUS Mg-Zn ALLOYS

We use a special ultrahigh-vacuum experimental setup which allows the preparation of the films by controlled coevaporation on sapphire substrates maintained at low temperature and the measurement of their optical properties (reflectance R and transmittance T), and their dc electrical resistance *in situ* between 10 and 370 K.²⁴ The base pressure in the experimental chamber is of the order of 10^{-9} Torr, and remains smaller than $5 \cdot 10^{-8}$ Torr during evaporation. The evaporation rates from the two separate crucibles are controlled by two calibrated quartz microbalances coupled with an Apple II Plus minicomputer; a feedback process allows monitoring of the heating of each crucible in order to keep constant the ratio of the deposition rates of the two constituents. Both the composition and the average mass thickness d_Q , defined as $d_Q = d_{Mg} + d_{Zn}$, d_{Mg} and d_{Zn} being deduced from the indications of the two quartz microbalances, with the Mg and Zn density taken to be equal to 1.74 and 7.14 g/cm³, respectively, can thus be determined with an uncertainty of $\pm 1\%$. The total deposition rate is in all cases of the order of 10 Å/sec.

The alloy composition has been checked by an α -particle backscattering technique;²⁵ the agreement with the quartz-microbalance indications is quite good, within a few percent.

The problem of the actual film thickness d was more difficult to solve. Due to the very rapid oxidization of the samples when submitted to ambient atmosphere, it proved impossible to measure d by our usual x-ray interference technique.²⁶ We therefore tried to determine the film thickness by using only the optical measurements performed *in situ* just after deposition. In a first method, d was taken as an additional adjustable parameter in the analysis of the near infrared data in terms of the Drude model; the results will be discussed in Sec. IV. The second method consisted of determining simultaneously the set of optical constants n_{i-1} , k_{i-1} , n_i , k_i , n_{i+1} , k_{i+1} ($n + ik$ being the complex refractive index), and the thickness d from the R , T , and δ_R values at three consecutive frequencies ω_{i-1} , ω_i , ω_{i+1} ; R and T are the measured film reflectance and transmittance and δ_R , phase change on re-

flection, is computed from the R data through a special application of the Kramers-Kronig dispersion relation.^{27,28} The "optical-thickness" values d_0 obtained by these two methods are in reasonable agreement with each other, but are systematically smaller than the "average-mass-thickness" values d_Q ; for example, for a film with $d_Q = 600$ Å, d_0 is found to be equal to 552 and 555 Å by the Drude method and the Kramers-Kronig method, respectively. The values of the alloy density for our coevaporated films, corresponding both to d_Q and to d_0 , are reported in Fig. 1 as a function of the Zn atomic concentration x_{Zn} . The density values obtained for bulk quenched alloys¹² are also indicated in this figure; the variation with x_{Zn} is identical, but the density is slightly smaller than for the coevaporated films. In the following, we will consider the optical thickness d_0 as the true film thickness. However, we will use both d_Q and d_0 for the analysis of the optical data in order to estimate the influence of the thickness value on the determination of the free-electron parameters.

The film reflectance and transmittance at nearly normal incidence are measured *in situ* with a special vacuum spectrophotometer, between 0.6 and 4.2 eV (2 and 0.3 μ m). The accuracy of these measurements is of the order of 0.1–0.3 %, which is absolutely necessary for a reliable analysis of the data. The measurements are performed just after deposition, as well as at different annealing stages if necessary. The complex dielectric constant $\tilde{\epsilon} = \epsilon_1 + i\epsilon_2 = (n + ik)^2$ is computed from the R and T values at any wavelength, using exact thin-film formulas and taking into account multiple reflections inside the transparent substrate; the thickness must be known for this procedure.²⁹

The dc electrical resistance is measured versus temperature between 10 and 370 K by a four-point method; the thermocouples are made of thin AuFe/chromel wires held in contact with the film surface with two indium patches. A special differential method, allowing the measurement of resistance changes as small as 10^{-3} Ω for resistance values greater than 100 Ω , is used when the sample resistance varies very little in temperature.

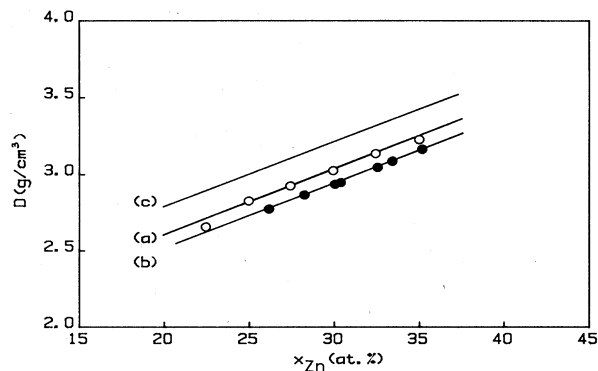


FIG. 1. Density of amorphous Mg-Zn alloys versus Zn concentration x_{Zn} : for quenched alloys, from Ref. 12(a); for coevaporated alloy films, if the film thickness is taken equal to the average mass thickness d_Q (b) or to the optical thickness d_0 (c).

We observed the amorphous alloy structure at room temperature using electron microscopy and electron diffraction, using pieces of the films detached from the substrate with collodion and collected on microscope grids after collodion dissolving. Unfortunately, due to the rapid oxidization of the films at ambient atmosphere, the diffraction patterns are difficult to analyze and no detailed structure study could be made.

III. dc ELECTRICAL RESISTIVITY

Amorphous Mg-Zn alloy films with thicknesses of the order of 550–700 Å and Zn concentrations ranging from 26 to 35 at. % were deposited at a constant deposition rate of about 10 Å/sec on sapphire substrates maintained at 10 K. The values of their dc electrical resistivity at the end of deposition ρ_e are comprised between 75 and 85 $\mu\Omega$ cm. As shown in Fig. 2, there is no significant variation of ρ_e with the alloy composition. When increasing temperature, ρ remains approximately constant over a small temperature range, up to about 30 K, then decreases slightly, goes through a plateau or a faint maximum around 150–200 K, and decreases again slowly above 200 K. The total relative variation of the resistivity between 10 and 300 K does not exceed 10%. This annealing behavior is illustrated in Fig. 3 for films with different compositions.

The films are still amorphous at room temperature, as confirmed by electron diffraction. Despite the superimposed oxide diffraction rings, the diffraction patterns clearly show an asymmetric broad first peak with a maximum at $q=4\pi(\sin\sigma)/\lambda=2.65\text{--}2.67$ Å, a characteristically split second peak with a maximum at $q\approx 4.4$ Å⁻¹, and a shoulder centered at $q\approx 4.9\text{--}5.1$ Å⁻¹. These results are in good agreement with those reported for bulk quenched alloys.^{11,12} Crystallization only occurs above room temperature, as shown in Fig. 3, by the steep decrease of the resistivity observed between 350 and 360 K. This crystallization temperature is in good agreement with those reported for quenched samples.^{30,31} It can be noted that the temperature coefficient of the resistivity of the crystalline phase is positive: $\approx 2 \times 10^{-3}$ K⁻¹, again in

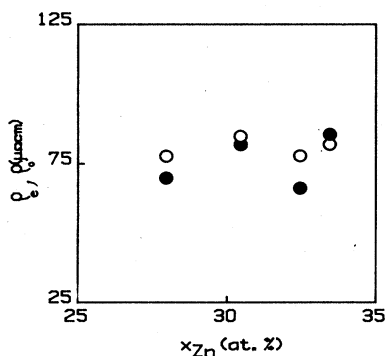


FIG. 2. dc electrical resistivity ρ_e (○), and optical resistivity ρ_0 (●), for as-deposited coevaporated amorphous Mg-Zn films with different compositions.

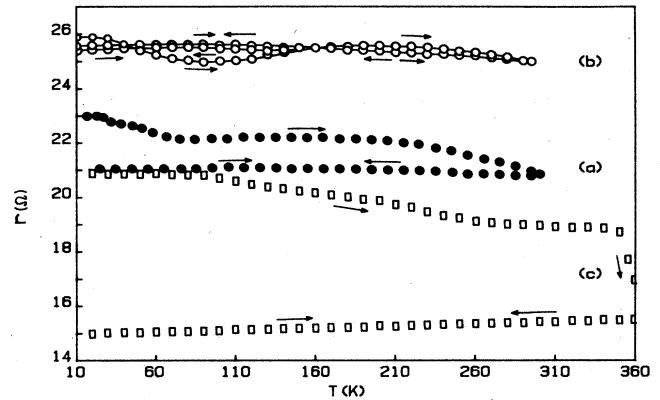


FIG. 3. Variation of the dc electrical resistance r with temperature T during annealing for coevaporated amorphous Mg-Zn alloy films: (a) $x_{Zn}=30.5$ at. %, (b) $x_{Zn}=33.5$ at. %, both deposited at 10 K; (c) $x_{Zn}=35$ at. %, deposited at 77 K; this last film has been annealed up to crystallization.

agreement with previous results.³⁰ The diffraction patterns after crystallization allow us to identify the already described $Mg_{51}Zn_{20}$ crystalline phase.^{30,32}

The complicated shape of the annealing curves $\rho(T)$ between 10 and 300 K indicates that the structural relaxation of amorphous Mg-Zn alloy films, deposited by coevaporation on low-temperature substrates, takes place in several successive steps, resulting either in a decrease (at about 30 K and above 200 K) or in an increase (around 150–200 K) of the resistivity. The process observed at intermediate temperatures (100–200 K) seems to be the most sensitive to the particular deposition conditions, and could concern medium-range inhomogeneities.

The reversible variation of the resistivity versus temperature between 10 and 300 K for amorphous Mg-Zn alloy films stabilized by annealing at room temperature is shown in a few cases in Fig. 4. ρ varies very little over the whole temperature range. It starts to increase very lightly, goes through a faint, broad maximum, then decreases until room temperature, the variation being approximately linear. These results are at least in qualitative agreement with those reported for bulk quenched amorphous alloys.^{12,15–17} The shallow minimum around 10 K pointed out by Matsuda and Mizutani¹⁵ can be detected for one sample. We also observe the T^2 dependence predicted at low temperatures by the extensions of the Faber-Ziman theory^{9,33} over a small temperature range below the maximum, as well as the empirical law: $\rho=\rho_{max}-A(T-T_{max})^{3/2}$ proposed by Matsuda and Mizutani¹⁵ above the maximum, before the approximately linear variation sets in. The different quantities characteristic of the resistivity behavior of the coevaporated amorphous alloys are summarized in Table I for different compositions. When comparing these results to those reported for quenched alloys, the following can be noted:

(i) The resistivity values are significantly larger than those corresponding to quenched alloys, which are usually comprised between 40 and 60 $\mu\Omega$ cm,^{14–18} but smaller

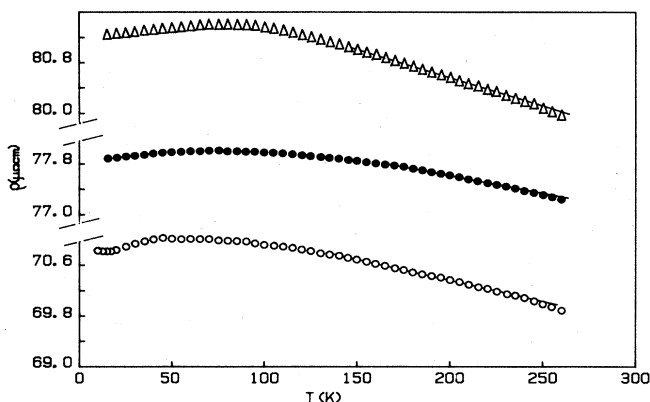


FIG. 4. Reversible variation with temperature T of the dc electrical resistivity of coevaporated amorphous Mg-Zn alloy films deposited at low temperature and annealed at room temperature: $x_{\text{Zn}} = 33.5$ at. % (Δ), 30.5 at. % (\bullet), 28 at. % (\circ).

than those of cosputtered films, comprised between 100 and $130 \mu\Omega \text{ cm}$.¹³

(ii) The position of the maximum, although varying somewhat from sample to sample irrespective of the composition, seems to be shifted to higher temperatures with respect to that in quenched samples ($\approx 50 \text{ K}$).

(iii) The temperature coefficient of the resistivity estimated in the 150–250 K range has somewhat smaller absolute values than that in quenched samples ($\approx 2 \times 10^{-4} \text{ K}^{-1}$).

Several rather sophisticated theoretical treatments, which are all based on the diffraction model, i.e., the generalization of the Faber-Ziman theory to amorphous systems, have been proposed recently in order to interpret the results of transport experiments on such low-resistivity amorphous alloys.^{34–39} They only differ in the handling of the different ingredients entering the Faber-Ziman theory. All treatments succeed in reproducing the general behavior of the dc electrical resistivity as a function of temperature. This proves that the diffraction model, which is basically a weak-scattering theory, is well adapted to such systems with resistivities smaller than $100 \mu\Omega \text{ cm}$. The theoretical values of the resistivity, of the order of $43 \mu\Omega \text{ cm}$ for amorphous Mg-Zn alloys,^{37,38} are in

good agreement with the lowest experimental values obtained for quenched samples. As for the exact $\rho(T)$ variation, these *ab initio* calculations clearly show that it is the result of a rather delicate interplay of structural, electronic, and dynamical variables;³⁸ this is particularly the case for the location and relative intensity of the low-temperature maximum, and for the slope in the vicinity of room temperature. All treatments emphasize the dramatic effect of the choice of the potential. On the other hand, factors such as the Fermi wave vector and the packing fraction influence not only the magnitude of the resistivity, but also the shape of the $\rho(T)$ curve, and could play a role in the scattering of the data relative to differently prepared samples. Despite the success of these models, some discrepancies with the experimental results concerning, for example, the composition dependence of the resistivity, or the thermopower behavior, suggest that the electronic transport properties of the amorphous alloys are not fully taken into account. It may be worth noting that the resistivity data obtained for coevaporated films vary appreciably from sample to sample. This suggests that films prepared by condensation of a mixed vapor on a cold substrate present “defects” contributing to the electron scattering mechanisms, in variable proportion depending on the peculiar deposition conditions. These defects could be related to fluctuations of both chemical and topological medium-range order.

IV. OPTICAL PROPERTIES

The complex dielectric constant of coevaporated amorphous Mg-Zn films, as determined at 10 K under ultrahigh vacuum immediately after deposition, appears to follow a free-electron-like behavior over most of the spectral range investigated. This is illustrated in Fig. 5, which shows the ϵ_1 and ϵ_2/λ spectra (ϵ_2/λ being related to the optical absorption) obtained for a film with $x_{\text{Zn}} = 30.5$ at. %, using the two thickness values $d_0 = 555 \text{ \AA}$ and $d_Q = 600 \text{ \AA}$.

We assume that the optical properties of the amorphous Mg-Zn alloys can be represented, at least in the near infrared, by the nearly-free-electron Drude model. We therefore tried to analyze the experimental complex dielectric constant with the expression

TABLE I. Quantities characteristic of the dc electrical resistivity behavior for coevaporated amorphous Mg-Zn alloy films with different compositions: ρ values at 10 K before and after annealing, and at 300 K; ratio of the maximum value to the room-temperature value $\rho_{\text{max}}/\rho_{300 \text{ K}}$; slope A of the plot: $\rho = \rho_{\text{max}} - A(T - T_{\text{max}})^{3/2}$; temperature of the maximum T_{max} ; temperature coefficient $\alpha = (1/\rho)(d\rho/dT)$ as determined in the 150–250 K range.

$\text{Mg}_{1-x}\text{Zn}_x$ at. %	$\rho^{10 \text{ K}}$		$\rho_{300 \text{ K}}$	$\rho_{\text{max}}/\rho_{300 \text{ K}}$	A ($10^{-4} \mu\Omega \text{ cm K}^{-3/2}$)	T_{max}	α (10^{-4} K^{-1})
	as-deposit ($\mu\Omega \text{ cm}$)	annealed 300 K ($\mu\Omega \text{ cm}$)					
28	78.5	72.5	69.5	1.023		45	-1.4
30.5	85	78	76.8	1.015	3	80	-0.7
32.5	78	72.7	70.7	1.024	10	90	-1.1
33.5	82	81	79.6	1.023	8	85	-1.2

$$\tilde{\epsilon} = P - \frac{\lambda^2}{\lambda_0^2} \frac{1}{1 + i(\lambda/\lambda_\tau)}$$

where $\lambda_0 = 2\pi c/\omega_p$, $\omega_p = (4\pi N_{\text{eff}}e^2/m_0)^{1/2}$ the plasma frequency of the nearly-free-electron gas with an effective

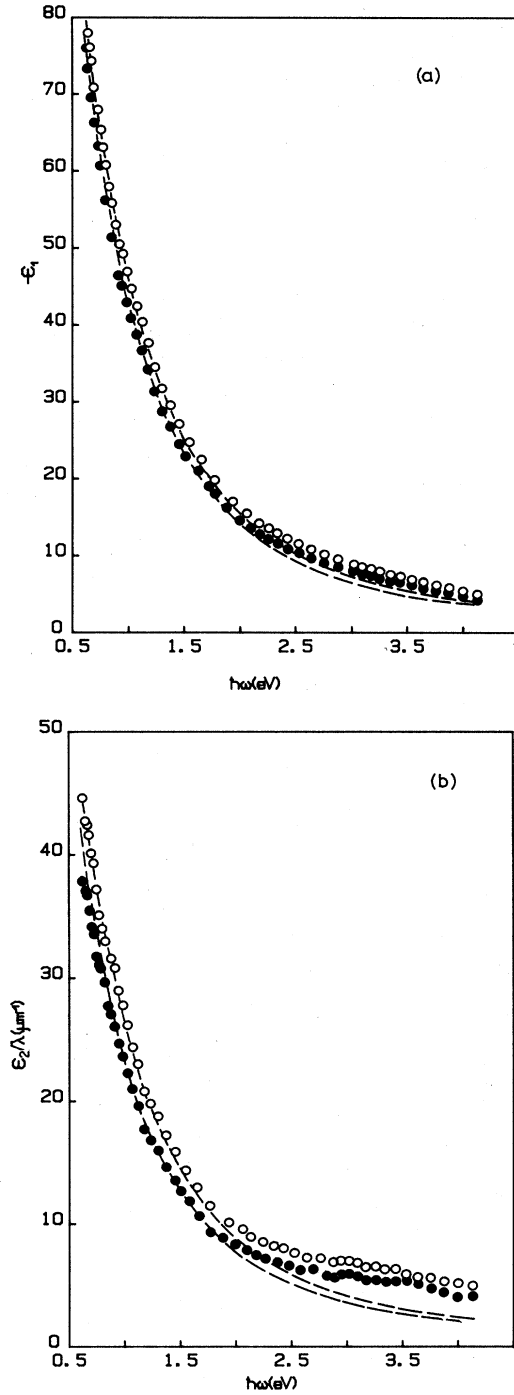


FIG. 5. Real part of the dielectric constant ϵ_1 (a) and optical absorption ϵ_2/λ (b) versus energy for a coevaporated amorphous Mg-Zn alloy film with $x_{\text{Zn}} = 30.5$ at.%, as computed with $d_Q = 600 \text{ \AA}$ (\bullet) and $d_0 = 555 \text{ \AA}$ (\circ); the dashed curves correspond to Drude fits in the 0.6–2 eV spectral range.

number per unit volume N_{eff} and an optical effective mass m_0 , and $\lambda_\tau = 2\pi c\tau_0$, τ_0 being the optical relaxation time of the conduction electrons, assumed to be independent on frequency. The real term P , which is equal to $1 + (\epsilon_a - 1) + \delta\epsilon_1^b$, accounts for the core polarization ($\epsilon_a - 1$), and for the contribution of interband transitions which may occur at higher energies:

$$\delta\epsilon_1^b = \frac{2}{\pi} \int_0^\infty \frac{\omega'\epsilon_2(\omega')}{\omega'^2 - \omega^2} d\omega'$$

This contribution can be considered as a constant for $\omega \ll \omega_b$, ω_b being the onset of interband transitions.

We used a least-squares-fitting procedure, with λ_0 , λ_τ , and P as adjustable parameters. Due to the problems encountered in the determination of the actual film thickness, we also considered d as an additional adjustable parameter. The fits were tried both directly on the (R, T) data and on the computed (ϵ_1, ϵ_2) data, over spectral ranges of increasing width towards high energies. Besides the root-mean-square deviation per point Σ , our program provided the asymptotic correlation matrix of the parameters. Figures 5 and 6 show a comparison between the experimental (ϵ_1, ϵ_2) and (R, T) values and the computed values corresponding to three-parameter Drude fits in the 0.6–2 eV spectral range, for a film with $x_{\text{Zn}} = 30.5$ at. % and $d_Q = 600 \text{ \AA}$ ($d_0 = 555 \text{ \AA}$). The optical data follow remarkably well the nearly-free-electron model with a constant relaxation time, from 0.6 to about 1.8 eV. At higher energies, the optical absorption ϵ_2/λ takes slightly larger values, while the deviation remains very small for ϵ_1 . The λ_0 and λ_τ values depend little on the spectral range chosen for the fit, as long as it does not extend beyond 2 eV, and they can be determined with a relative uncertainty of a few per cent. In contrast, the P values can vary appreciably with the type of fit, but they remain small, roughly between 0 and 1. We checked the reliability of the λ_0 and λ_τ values obtained by this curve-fitting procedure by com-

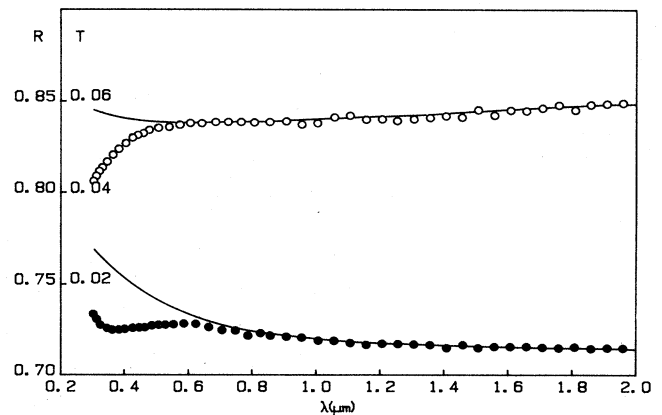


FIG. 6. Reflectance R (\circ) and transmittance T (\bullet) vs wavelength λ between 0.3 and 2 μm for the same film as in Fig. 5 ($d_Q = 600 \text{ \AA}$, $x_{\text{Zn}} = 30.5$ at. %); the continuous curves correspond to the Drude fit.

paring them to those determined graphically via the following relations, easily deduced from the Drude expression:

$$\frac{\epsilon_2}{\lambda} = \frac{1}{\lambda_\tau} (P - \epsilon_1),$$

$$\left[\frac{\epsilon_2}{\lambda} \right]^{-1} = \frac{\lambda_0^2 \lambda_\tau}{\lambda^2} + \frac{\lambda_0^2}{\lambda_\tau}.$$

Such a graphical determination is presented in Fig. 7 for the same film as in Figs. 5 and 6 ($d_Q = 600 \text{ \AA}$); the corresponding parameter values $\lambda_0 \approx 0.155 \text{ \mu m}$, $\lambda_\tau \approx 1.90 \text{ \mu m}$, $P \approx 1$, are in good agreement with the Drude fit values: $\lambda_0 = 0.156 \text{ \mu m}$, $\lambda_\tau = 1.85 \text{ \mu m}$. The determination of the optical thickness as a fourth adjustable parameter was only possible in a few cases, due to a strong correlation between λ_0 and both λ_τ and d . As already emphasized, the obtained values were always consistent with the Kramers-Kronig values, and definitely smaller than the corresponding mass thickness values.

The values of the parameters λ_0 and λ_τ (as well as the corresponding $\hbar\omega_p$ and \hbar/τ_0 values) determined for amorphous Mg-Zn alloys with Zn concentrations varying from 28 to 33.5 at. %, are summarized in Table II and Fig. 8. Only the values corresponding to the assumed true film thickness d_0 have been retained in the table, but the figure presents the results obtained with both thickness values d_Q and d_0 . We have also reported in Table II the values of the average effective number of conduction electrons per atom n_{eff} computed from λ_0 by assuming an optical effective mass equal to the free-electron mass (these values are displayed in Fig. 9), as well as the values of the ratio of the optical effective mass to the free-electron mass m_0/m computed from λ_0 by assuming an average effective number of conduction electrons per atom equal to 2, which is the common valency of both constituents. We have eventually indicated, both in Table II and in Fig. 3, the values of the optical resistivity ρ_0 , defined as the reciprocal zero-frequency limit of the optical conductivity $\delta = \omega\epsilon_2/4\pi$, and given by:

$$\rho_0 = \frac{2}{c} \frac{\lambda_0^2}{\lambda_\tau} = \frac{m_0}{N_{\text{eff}} e^2 \tau_0}.$$

These results call for the following comments:

(a) The values of λ_0 are significantly larger than those expected from a free-electron model in which each constituent would contribute two electrons to the alloy conduction band, with an optical effective mass equal to the free-electron mass; for example, for $x_{\text{Zn}} \approx 30$ at. %, the

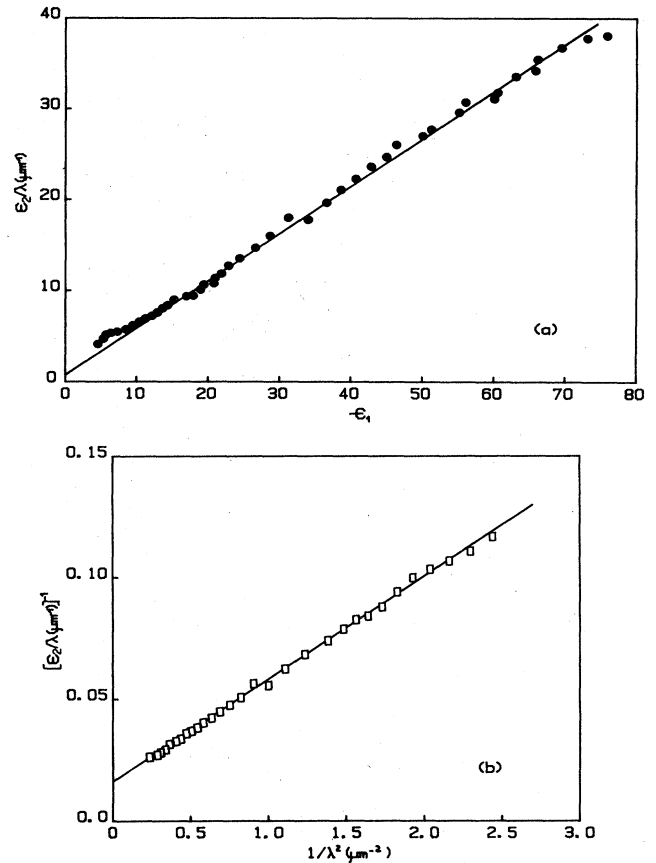


FIG. 7. Graphical test of the Drude model for the same film as in Figs. 5 and 6, using $d = d_Q = 600 \text{ \AA}$: (a) ϵ_2/λ vs $-\epsilon_1$; (b) $(\epsilon_2/\lambda)^{-1}$ vs λ^{-2} .

predicted free-electron value of λ_0 should be of the order of 0.107 \mu m , while the experimental value is of the order of 0.150 \mu m . The difference definitely exceeds any possible experimental uncertainty. If we try to fit the optical data with the Drude model, with λ_0 fixed at the free-electron value and d taken as an adjustable parameter, the obtained d value is unreasonably too small, for example, $d = 391 \text{ \AA}$, compared to $d_Q = 600 \text{ \AA}$ in the case of the film already discussed. This discrepancy between the experimental λ_0 value and the value predicted by a simple free-electron model can be interpreted as due either to a value of the effective average number of conduction elec-

TABLE II. Values of the free-electron parameters as deduced from the Drude analysis of the optical data for amorphous Mg-Zn alloys with different compositions (see text for the definitions).

Mg-Zn	x_{Zn} (at. %)	λ_0 (μm)	$\hbar\omega_p$ (eV)	n_{eff}	m_0/m	λ_τ (μm)	\hbar/τ_0 (eV)	ρ_0 ($\mu\Omega\text{cm}$)
9	28	0.148	8.38	0.98	2.04	1.88	0.66	77.7
5	30.5	0.148	8.38	0.97	2.05	1.78	0.70	82.0
7	32.5	0.142	8.73	1.05	1.90	2.02	0.61	66.5
6	33.5	0.140	8.86	1.08	1.85	1.53	0.81	85.4

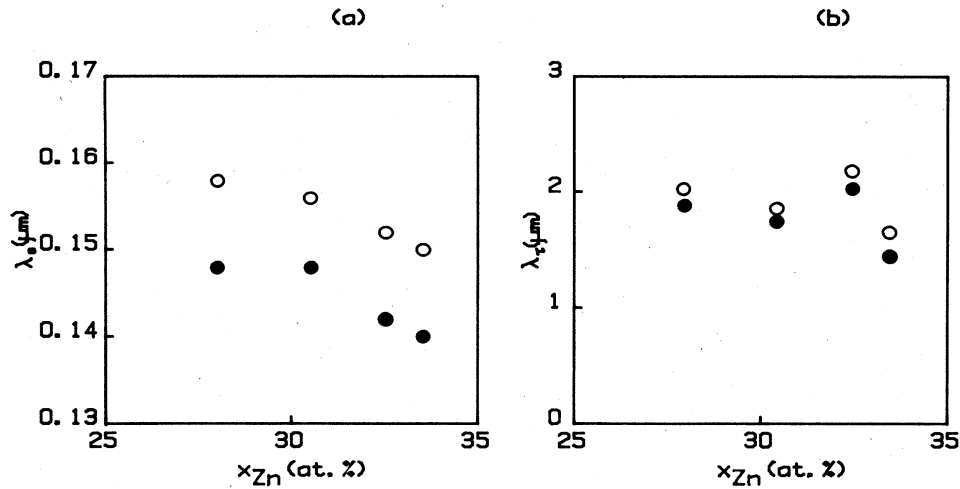


FIG. 8. Values of the plasma wavelength λ_0 (a) and of the relaxation wavelength λ_r (b) vs atomic Zn concentration x_{Zn} for co-evaporated amorphous Mg-Zn alloy films, as deduced from the Drude analysis of the optical data, with $d = d_0$ (\circ) and $d = d_0$ (\bullet).

trons per atom, as deduced from the optical properties, much smaller than 2, or to an enhancement of the optical effective mass of the conduction electrons with respect to the free-electron mass. The first interpretation is in contradiction with the results of Hall-constant measurements on quenched amorphous Mg-Zn alloys,¹² which give an average number of conduction electrons per atom of the order of 2, varying only slightly with composition (these values are also reported in Fig. 9), as well as with those of Compton profile²⁰ and electronic specific-heat coefficient¹⁸ experiments, which both yield a Fermi wave vector k_F in good agreement with the predicted free-electron value. The second interpretation, in terms of optical mass enhancement, has previously been chosen to explain similar discrepancies observed between the optical results and

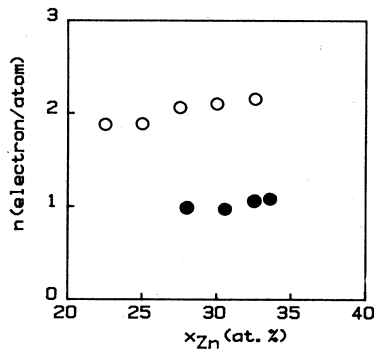


FIG. 9. Average number of conduction electrons per atom n vs atomic Zn concentration x_{Zn} for amorphous Mg-Zn alloys: (\circ) deduced from Hall-constant measurements on quenched alloys (Ref. 12); (\bullet) deduced from the Drude analysis of the optical data obtained on coevaporated alloy films (with an effective mass equal to the free-electron mass).

the predictions of a free-electron model, in the case of free-electron-like amorphous Sn-Cu and Sn-Au alloys.²² The ratio m_0/m was found to be comprised between about 1.6 and 1.7 for Sn-Cu and between 1.8 and 1.4 for Sn-Au, for noble metal concentrations varying from 20 to 80 at. %.

(b) The values of λ_r are comprised between 1.5 and 2.5 μm , which corresponds to \hbar/τ_0 values comprised between 0.8 and 0.5 eV. These values seem to depend rather sensitively on the peculiar film structure, so that their variation with the alloy composition cannot be clearly established. The optical relaxation times in amorphous Mg-Zn alloys are significantly larger than in similarly prepared amorphous Au-Ge and Ag-Ge alloys,²³ or amorphous Au-Sn and Cu-Sn alloys,²² which is consistent with the lower resistivities of these alloys. The corresponding mean free paths are of the order of 15–20 Å, which is appreciably larger than the interatomic distances, so that a free-electron model can be justified.

(c) The optical resistivity ρ_0 deduced from the optical parameters λ_0 and λ_r is in all cases of the same order of magnitude as the dc electrical resistivity ρ_e . This is an additional argument in favor of the use of a free-electron model for the analysis of the optical data. The difference between ρ_0 and ρ_e , which varies from sample to sample, can probably only be attributed to experimental uncertainties on the optical data.

V. CONCLUSION

We have succeeded in preparing amorphous Mg-Zn alloys in the form of thin films by coevaporation under ultrahigh vacuum on sapphire substrates maintained at low temperature (≈ 10 K) for Zn concentrations ranging from 26 to 35 at. %. The samples can be annealed *in situ* up to room temperature while remaining amorphous; they crystallize at about 350 K, like quenched bulk alloys. The dc

electrical resistivity and the optical properties between 0.6 and 4 eV of these amorphous alloy films have been investigated *in situ* in order to avoid contamination. The behavior of their resistivity versus temperature is found to be similar to the one reported for quenched bulk alloys, with only small differences in the details of the curves, i.e., in the location of the maximum, slope of the high-temperature part, etc., and it can be well interpreted in the framework of the diffraction model. However, the absolute values of the resistivity are significantly higher than those for quenched alloys. This suggests that thin films, even after annealing at room temperature, contain defects, probably related to medium-range inhomogeneities, which may contribute to the electron scattering.

The analysis of the optical properties unambiguously shows that the complex dielectric constant follows remarkably well the free-electron Drude model with a constant optical relaxation time τ_0 , at least at low energies and up to about 1.8 eV. The optical resistivity, computed from the conduction-electron parameters deduced from the Drude analysis of the optical data, is in all cases very close to the dc electrical resistivity, which supports the validity of the model and the consistency of the analysis. The \hbar/τ_0 values are comprised between 0.5 and 0.8 eV, and seem to be more sensitive to the film structure than to its composition. They are significantly smaller in these amorphous alloys between two simple metals than in other free-electron-like amorphous alloys involving noble metals, which can be traced back to the fact that their conduction electrons have essentially *s* and *p* character. The Drude analysis also yields the values of the ratio of the average number of conduction electrons per atom to their optical effective mass. These values are definitely smaller than those expected from the free-electron model with an optical mass equal to the free-electron mass, which creates a serious problem. Since both the number of conduction electrons per unit volume and the density of states at the Fermi level are known to be close to the free-electron values from other experiments, one must admit that the optical effective mass is much larger than the free-electron mass: $m_0/m \simeq 2$. Values of m_0/m larger

than 1 are also systematically found for crystalline polyvalent metals.^{40,41} In this case, they are well explained, on the basis of the sum rule:

$$\frac{m}{2\pi^2 e^2} \int_0^\infty \omega \epsilon_2^{\text{interband}}(\omega) d\omega + N \frac{m}{m_0} = N_{\text{total}}$$

(with N_{total} the total electron density and N the number of conduction electrons per unit volume), by a transfer of oscillator strength from intraband transitions of the conduction electrons to "parallel-band" interband transitions of these same electrons, connected with the perturbations of the free-electron band by Bragg reflection planes (Brillouin-zone planes).⁴²⁻⁴⁴ Such an interpretation is difficult to retain in the absence of long-range order, but we can keep the idea of a transfer of oscillator strength because of interband transitions, whatever the origin of the latter. The deviations observed at high energies between the experimental complex dielectric constant and the Drude model could be an indication for such transitions.

It may also be worth recalling that photoemission and soft-x-ray emission experiments performed on the parent CaAl amorphous alloys have revealed unexpected structures in the total valence-band density of states, as well as a striking modification of the Al *p* partial density of occupied states with respect to pure Al.⁴⁵ Computations on Ca_{0.75}Al_{0.25} with the Cu₃Au structure have, on the other hand, predicted a splitting of the valence band.⁴⁵ It would be very interesting to determine whether the valence band of amorphous Mg-Zn alloys also exhibits strong deviations from a free-electron band. If it was indeed the case, the application of the Drude model, which is as a rule strictly valid for a free-electron gas only, could lead to incorrect results concerning the conduction-electron behavior.

ACKNOWLEDGMENT

The authors acknowledge partial support from the European Office of Aerospace Research and Development.

*Unite' Associee au Centre National de la Recherche Scientifique No. 040-781.

¹J. Hafner and L. Von Heimendahl, *Phys. Rev. Lett.* **42**, 386 (1979).

²J. Hafner, *J. Phys. (Paris) Colloq.* **41**, C8-139 (1980).

³J. Hafner, *Phys. Rev.* **21**, 406 (1980).

⁴S. M. Mujibur Rahman, *Z. Phys. B* **45**, 307 (1982).

⁵J. M. Ziman, *Philos. Mag.* **6**, 1013 (1961).

⁶T. E. Faber and J. M. Ziman, *Philos. Mag.* **11**, 153 (1965).

⁷T. E. Faber, *Theory of Liquid Metals* (Cambridge University Press, London, 1972).

⁸G. Baym, *Phys. Rev. A* **135**, 1691 (1964).

⁹K. Froböse and J. Jäckle, *J. Phys. F* **7**, 2331 (1977).

¹⁰J. Jäckle and K. Froböse, *J. Phys. F* **9**, 967 (1979).

¹¹A. Calka, M. Madhava, D. E. Polk, B. C. Giessen, H. Matyja, and J. Vander Sande, *Scr. Metall.* **11**, 65 (1977).

¹²T. Matsuda and U. Mizutani, in *Proceedings of the 4th Inter-*

national Conference on Rapidly Quenched Metals, edited by T. Masumoto and K. Susuki (Japan Institute of Metals, Sendai, 1982), p. 1315.

¹³J. J. Hauser and J. Tauc, *Phys. Rev. B* **17**, 3371 (1978).

¹⁴J. Hafner, E. Gratz, and H. J. Güntherodt, *J. Phys. (Paris) Colloq.* **41**, C8-512 (1980).

¹⁵T. Matsuda and U. Mizutani, *J. Phys. F* **12**, 1877 (1982).

¹⁶M. N. Baibich, W. B. Muir, Z. Altounian and Tu Guo-Hua, *Phys. Rev. B* **26**, 2963 (1982).

¹⁷G. Fritsch, J. Willer, A. Wildermuth, and E. Luscher, *J. Phys. F* **12**, 2965 (1982).

¹⁸U. Mizutani and T. Mizoguchi, *J. Phys. F* **11**, 1385 (1981).

¹⁹B. C. Giessen, A. Calka, R. Raman, and D. J. Sellmyer, in *Proceedings of the Second International Symposium on Amorphous Magnetism*, edited by R. A. Levy and R. Hasegawa (Plenum, New York, 1977), p. 197.

²⁰N. Shiotani, N. Sakai, H. Sekizawa, and T. Mizoguchi, *J.*

- Phys. Soc. Jpn. **50**, 828 (1981).
- ²¹E. Hauser, R. J. Zircke, J. Tauc, J. J. Hauser, and S. R. Nagel, *Phys. Rev. Lett.* **40**, 1733 (1978); *Phys. Rev. B* **19**, 6331 (1979).
- ²²D. Korn and H. Pfeifle, *J. Phys. F* **9**, 1175 (1979).
- ²³M. L. Theye, V. Nguyen-Van, and S. Fisson, *Philos. Mag. B* **47**, 31 (1983).
- ²⁴V. Nguyen-Van and S. Fisson, *Rev. Phys. Appl.* **13**, 155 (1978).
- ²⁵J. P. Dupin (private communication).
- ²⁶H. Kiessig, *Ann. Phys. (Leipzig)* **10**, 769 (1931).
- ²⁷C. Froissart, *Optica Acta* **16**, 45 (1969).
- ²⁸C. Perrin (private communication).
- ²⁹F. Abeles and M. L. Thèye, *Surf. Sci.* **5**, 325 (1966).
- ³⁰N. Shiotani, H. Narumi, H. Arai, K. Wakatsuki, Y. Sasa, and T. Mizoguchi, in *Proceedings of the 4th International Conference on Rapidly Quenched Metals*, edited by T. Masumoto and K. Susuki (Japan Institute of Metals, Sendai, 1982) p. 667.
- ³¹T. Mizoguchi, H. Narumi, N. Akutsu, N. Watanabe, N. Shiotani, and M. Ito, *J. Non-Cryst. Solids* **61/62**, 285 (1984).
- ³²I. Higashi, N. Shiotani, M. Uda, T. Mizoguchi, and H. Katoh, *J. Solid State Chem.* **36**, 225 (1981).
- ³³L. V. Meisel and P. J. Cote, *Phys. Rev. B* **17**, 4652 (1978).
- ³⁴L. V. Meisel and P. J. Cote, *Phys. Rev. B* **27**, 4617 (1983).
- ³⁵P. J. Cote and L. V. Meisel, *J. Non-Cryst. Solids* **61/62**, 1167 (1984).
- ³⁶L. V. Meisel and P. J. Cote, *J. Non-Cryst. Solids* **61/62**, 1307 (1984).
- ³⁷J. Laakkonen and R. M. Nieminen, *J. Phys. F* **13**, 2265 (1983).
- ³⁸J. Hafner, *J. Non-Cryst. Solids* (to be published).
- ³⁹J. Hafner, *J. Phys. F* **14**, 1685 (1984).
- ⁴⁰G. P. Motulevich, *Usp. Fiz. Nauk.* **97**, 211 (1969) [*Sov. Phys.—Usp.* **12**, 80 (1969)].
- ⁴¹A. G. Mathewson and H. P. Myers, *J. Phys. F* **2**, 403 (1972).
- ⁴²H. Ehrenreich, H. R. Phillip, and B. Segall, *Phys. Rev.* **132**, 1918 (1963).
- ⁴³W. A. Harrison, *Phys. Rev.* **147**, 467 (1966).
- ⁴⁴N. W. Ashcroft and K. Sturm, *Phys. Rev. B* **3**, 1898 (1971).
- ⁴⁵S. R. Nagel, U. M. Gubler, C. F. Hague, J. Krieg, R. Lapka, P. Oelhafen, H. J. Güntherodt, J. Evers, A. Weiss, V. L. Moruzzi, and A. R. Williams, *Phys. Rev. Lett.* **49**, 575 (1982).